Adhesion between a viscoelastic material and a solid surface

F. Saulnier[1*], T. Ondarçuhu[2†], A. Aradian[1,3‡] and E. Raphaël[1§]

[1]Laboratoire de Physique de la Matière Condensée UMR CNRS 7125

and Fédération de Recherche Matière et Systèmes Complexes FR CNRS 2438,

Collège de France, 11, place Marcelin Berthelot, 75231 Paris Cedex 05, France

[2] Centre d'Elaboration des Matériaux et d'Etudes Structurales (CEMES), U.P.R. CNRS 8011,

29, rue Jeanne Marvig, 31055 Toulouse Cedex 4, France.

[3] University of Edinburgh, School of Physics,King's Buildings JCMB,

Edinburgh EH9 3JZ, United Kingdom.

February 1, 2008

Abstract

In this paper, we present a qualitative analysis of the dissipative processes during the failure of the interface between a viscoelastic polymer, characterized by a weak adhesion, and a solid surface. We reassess the "viscoelastic trumpet" model [P.-G. de Gennes, C. R. Acad. Sci. Paris, **307**, 1949 (1988)], to express the viscous energy dissipated in the bulk as a function of the rheological moduli of the material, involving the local frequencies of sollicitation during crack propagation. We deduce from this integral expression the dhesion energy for different kind of materials: (i) we show that, for a crosslinked polymer, the dissipation had been underestimated at low velocities. Indeed, the interface toughness $G(V)$ starts from a relatively low value, G_0, daue to local processes near the fracture tip, and rises up to a maximum of order $G_0(\mu_\infty/\mu_0)$ (where μ_0 and μ_∞ stand for the elastic modulus of the material, respectively at low and high strain frequencies). This enhancement of fracture energy is due to far-field viscous dissipation in the bulk material, and begins for peel-rates V much lower than previously thought. (ii) For a polymer melt, the adhesion energy is predicted to scale as $1/V$. In the second part of this paper, we compare some of these latest theoretical predictions with experimental results about the viscoelastic adhesion between a polydimethylsiloxane polymer melt and a glass surface. In particular, the expected dependence of the fracture energy versus separation rate is confirmed by the experimental data, and the observed changes in the concavity of the crack profile are in good agreement with our simple model. More generally, beyond the qulitative and simple picture used for our approach, we expect our theoretical treatment to apply for relatively *weak viscoelastic adhesives*, for which the crack-tip dissipative term G_0 is weakly dependent on the fracture velocity.

---

[*]florent.saulnier@college-de-france.fr

[†]ondar@cemes.fr

[‡]A.Aradian@ed.ac.uk

[§]elie.raphael@college-de-france.fr

1 Introduction

Understanding how the interface between a polymer and another material fails is important for many industrial applications and has therefore been the subject of many studies in the last 30 years[1–3]. A quantity of central interest is the *interface toughness* (also called the adhesion energy), G, which is the energy per unit area needed to make a crack separating the two materials travel along the interface. If the polymer is above its glass transition temperature, this energy is dissipated - as the crack advances - by both local processes (occurring near the crack tip) and viscoelastic losses (taking place over macroscopic volumes)[4]. Some years ago, Gent and Schultz[5] and Andrews and Kinloch[6] showed that, for elastomeric adhesives, the variations of the interface toughness, G, with the crack velocity, V, can be written as:

$$G(V) = G_0(1 + \varphi(a_T V)), \tag{1}$$

where G_0 is the limiting value of the fracture energy at zero rate of crack growth, and represents local processes. According to Eq.(1), the contribution of the bulk viscoelastic losses, $G_v(V) = G(V) - G_0$, is given by $G_v(V) = G_0\varphi(a_T V)$ (where the temperature-shift factor a_T is given by the Williams-Landel-Ferry equation[7]) and is therefore itself proportional to the local contribution G_0. This remarkable fact was explained by de Gennes at the level of scaling laws[8,9], and further developed more rigorously by Hui, Xu and Kramer[10] (for other related studies, see[11–16]). In the first part of this paper, we reconsider de Gennes' model in the case of the interface between a poorly crosslinked elastomer (or a polymer melt) and a solid surface. We show, in particular, that the far-field viscoelastic contributions to the interface toughness play a significant role at separation rates much lower than previously thought. We also reconsider the profile of the crack[8], confirming some predictions of the earlier approach of Greenwood and Johnson[17]. In the second part of the paper we present experimental results for the adhesion between a polymer melt and a glass surface (for earlier work on "tack", see, *e.g.*, refs.[18–21]). These results for the fracture energy and the crack profile, which extend earlier work by Ondarçuhu[22], are then compared with the theoretical predictions of section 2.

2 Theoretical approach

2.1 Viscoelastic features of the polymer material

Many polymers are characterized by a viscoelastic behavior, exhibiting liquid-like or solid-like responses to mechanical sollicitations, depending on the frequency range of sollicitation. For the sake of simplicity, as in Refs.[8,10], we assume that the polymer material is characterized by a single relaxation time[23], τ , and that its rheological behavior can be described by a complex modulus $\underline{\mu}(\omega) = \mu'(\omega) + i\mu''(\omega)$ (we denote complex quantities with underlined variables), given by:

$$\underline{\mu}(\omega) = \mu_0 + (\mu_\infty - \mu_0)\frac{i\omega\tau}{1 + i\omega\tau}. \tag{2}$$

This expression 2 can depict both mechanical responses of crosslinked and uncrosslinked polymers, by taking in this last case $\mu_0 = 0$ (*i.e.* in the absence of low-frequency elastic
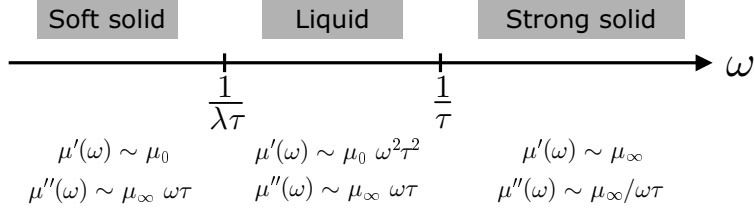
Figure 1: Viscoelastic features of a cross linked rubber: τ is the relaxation time, μ_0 is the elastic modulus at low frequencies ω, μ_∞ is the elastic modulus at high frequencies, and η is the viscosity of the liquid in the intermediate frequency range.

modulus). In the following, we will discuss both cases and will use a fundamental parameter, denoted λ, characterizing the ratio between high and low-frequency elastic moduli. For a poorly cross-linked elastomer, some chains are tied by one end only (some others might even be free): in this case, the low-frequency modulus μ_0 (related to the network) is small, while the high-frequency modulus μ_∞ (which contains the effects of the entangled free chains and of the dangling ends) is high. We will thus suppose that this ratio of modulus is high, as it can be typically achieved[24]:

$$\lambda \equiv \frac{\mu_\infty}{\mu_0} \sim 100. \tag{3}$$

Comparing the deformation rate with the relaxation time of the material, τ, *three* regimes can be distinguished, as summarized in Fig.1:

(i) At very low ω, *i.e.* $\omega < 1/(\lambda\tau)$, we have $\underline{\mu} \approx \mu_0$. The complex modulus is thus essentially real (*i.e.* $\mu' \gg \mu''$): the elastic component dominates, and the material can be considered a *soft solid*.

(ii) For $1/(\lambda\tau) < \omega < 1/\tau$, we have:

$$\underline{\mu}(\omega) \approx (\mu_\infty - \mu_0)i\omega\tau = i\omega\eta. \tag{4}$$

In this frequency range, where $\mu' \ll \mu''$, the rheology is mainly viscous-type: the material is a *liquid* with a viscosity $\eta = (\mu_\infty - \mu_0)\tau \sim \mu_\infty\tau$.

(iii) At high frequencies, *i.e.* $\omega > 1/\tau$, we find back a regime where $\mu' \gg \mu''$, and thus recover a *strong solid* with an elastic modulus $\mu \approx \mu_\infty$.

During crack propagation, the strain rate imposed to the material is high near the fracture tip, and lowers as the distance x to the head increases (far from the tip, the material had more time to relax the stresses). Following Ref.[9], we thus relate the distance x to the tip with the frequency ω by a simple scaling law of the form:

$$\omega \cong \frac{2\pi V}{x}. \tag{5}$$

As a consequence, we can distinguish three spatial regions in the bulk of the moving rubber, corresponding to the three regimes of frequencies defined above. In Fig.2 we present a simple view of the fracture profile when the crack propagates in a crosslinked polymer at speed V. Note
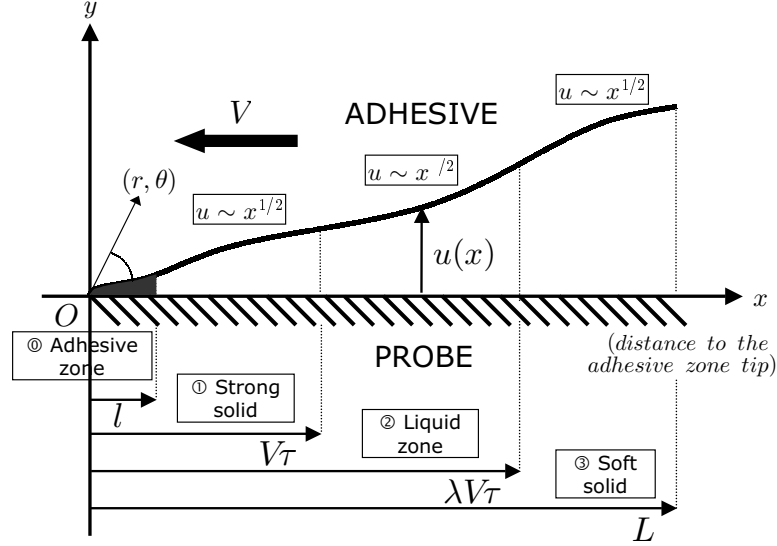
Figure 2: The "viscoelastic trumpet" model for a crosslinked elastomer characterized by a single relaxation time τ. By a simple relation between the distance to the fracture tip (x) and the frequency of deformation (ω), three regions with different viscoelastic properties can be distinguished. The adhesive zone is a region of length l where high stresses apply and give rise to irreversible dissipative processes. The moving frame (x, y) is centered at the adhesive zone tip, and (r, θ) is the associated polar coordinate system.

that this graphic representation corresponds to a velocity chosen in the range $l/\tau < V < L/\lambda\tau$, where L is the crack length[25].

Directly ahead the crack tip (located at $x = l$) is an adhesive zone of length l (assumed to be smaller than $1000\mathring{A}$), where local dissipative processes take place[26], and lead to the G_0 term of order 1 to 10 J·m^{-2}. In the following, all relevant dimensions of the problem (*e.g.* the crack length or the specimen dimensions in a fracture test) will be assumed to be sufficiently large compared with the adhesive zone size. For simplicity reasons, we will also suppose this length l constant and independent of separation rate V

Close to the fracture tip, the small spatial scales correspond to high rates of deformation: this region (number 1 in Fig.2 : $x < V\tau$) is a strong solid of elastic modulus μ_∞. At intermediate distances (region 2: $V\tau < x < \lambda V\tau$), the behavior is viscous-type: the polymer can be viewed a liquid of viscosity η. Far away the fracture head (region 3: $x > \lambda V\tau$), the material is a soft solid of modulus μ_0.

2.2 Integral expression for the fracture energy

A few years ago[9], de Gennes proposed a general relation between the energy $G_v(V)$ viscously dissipated during crack propagation at separation rate V, and the real ($\mu'(\omega) = \text{Re}[\underline{\mu}(\omega)]$) and imaginary ($\mu''(\omega) = \text{Im}[\underline{\mu}(\omega)]$) parts of the complex modulus $\underline{\mu}(\omega)$.

4

2.2.1 Viscous dissipation $G_v(V)$ in the polymer bulk

Let us begin with a general calculation of the energy dissipated in a viscoelastic material, within the framework of linear viscoelasticity and using the more convenient complex representation of the oscillatory motion. When the material is submitted to an oscillatory stress at frequency ω, characterized by its complex form $\underline{\sigma} = \sigma_0 \exp i\omega t$, the material response, given by the complex strain, $\underline{\gamma}$, is of the form:

$$\underline{\sigma} = \underline{\mu}(\omega)\underline{\gamma}. \tag{6}$$

The energy dissipated per unit of time, and per unit of volume, is given by $\sigma\dot{\gamma}$, where $\dot{\gamma}$ denotes the strain-rate. One can show that the time-averaged of this quantity, $\langle \sigma\dot{\gamma} \rangle$, is simply given by:

$$\langle \sigma\dot{\gamma} \rangle = \mathrm{Re}\left[\frac{\underline{\sigma} \cdot \underline{\dot{\gamma}}^*}{2}\right]. \tag{7}$$

Here, $\underline{\dot{\gamma}}^*$ is the complex conjugate of the complex strain-rate $\underline{\dot{\gamma}} = i\omega\underline{\gamma}$.

Using Eq.(6), we find that the viscous energy dissipated by the system depends on *both* loss (μ'') and storage (μ') modulus:

$$\mathrm{Re}\left[\frac{\underline{\sigma} \cdot \underline{\dot{\gamma}}^*}{2}\right] = \frac{\sigma_0^2}{2} \cdot \frac{\omega\,\mu''(\omega)}{\mu'(\omega)^2 + \mu''(\omega)^2}. \tag{8}$$

Let us now turn back to the trumpet model. The viscous dissipation $T\dot{S}$ (per unit length of the fracture line) is:

$$T\dot{S} = \int\int \langle \sigma\dot{\gamma} \rangle \,\mathrm{d}x\mathrm{d}y = \int\int \mathrm{Re}\left[\frac{\underline{\sigma} \cdot \underline{\dot{\gamma}}^*}{2}\right] \mathrm{d}x\mathrm{d}y. \tag{9}$$

In our model, we assume that the stress amplitude is given by $\sigma_0 = K_I/\sqrt{r}$ (cf. part 2.3 for precisions). We can also relate the distance to crack tip r to local frequencies of excitation ω by the scaling relation (5): $\omega(r) = V/r$. The integrand inside the right-hand side of Eq.(9) thus depends only on r, and we can replace the integral over x and y (on the half-space $y \geqslant 0$) by an integral over r (from $r = l$ to $r \sim L$), omitting numerical coefficient due to the integration over θ (from 0 to π):

$$T\dot{S} \cong \int \sigma_0^2 \frac{\omega\,\mu''(\omega)}{\mu'(\omega)^2 + \mu''(\omega)^2}\bigg|_{\omega=V/r} r\mathrm{d}r. \tag{10}$$

Using relation (5), we turn the Eq.(10) into an integral over frequencies of solicitation:

$$T\dot{S} \cong -K_I^2 V \int \frac{\mu''(\omega)}{\mu'(\omega)^2 + \mu''(\omega)^2} \frac{\mathrm{d}\omega}{\omega}. \tag{11}$$

The viscous dissipation $T\dot{S}$ and G_v are simply related by $T\dot{S} = VG_v$. Finally, as the fracture energy at zero velocity G_0 and the applied stress intensity factor K_I are related by the classical expression $G_0 = K_I^2/\mu_\infty$, we end up with[9]:

$$\frac{G_v(V)}{G_0} \cong \mu_\infty \int_{\omega_{min}}^{\omega_{max}} \frac{\mu''(\omega)}{\mu'(\omega)^2 + \mu''(\omega)^2} \frac{\mathrm{d}\omega}{\omega}. \tag{12}$$

G_0 is the adhesion energy due to local processes near the tip. The limiting values $\omega_{min} = V/L$ and $\omega_{max} = V/l$ define the range of frequency over which the material is excited.

The analytical results derived from Eq.(12) are presented in the appendix. Using the form (2) of the complex modulus of the material, the evolution of the total adhesion energy $G = G_0 + G_v$ versus crack velocity can be predicted for both cases of crosslinked and uncrosslinked ($\mu_0 = 0$) polymers. For the sake of conciseness, we will only qualitatively discuss the contribution of the different zones for G_v, which contrasts with some predictions of the classical picture of viscoelastic trumpet.

2.2.2 Contribution of the different zones for the adhesion energy

It was pointed out in a preceding paper[9] that the dissipation in the liquid zone predominates for the overall dissipation (because the liquid region is huge, ranging from $V\tau$ to $\lambda V\tau$). This gives rise to amplification of the adhesion energy by a factor λ ($G = \lambda G_0$) when the separation rate is taken between l/τ and $L/\lambda\tau$. This domain of velocities corresponds to a fully developed liquid zone, which explains the maximum of fracture energy (as the other "elastic" zones do not dissipate energy in this simple view).

In fact, it is worth noting that this enhancement begins for *much lower separation rates*. In order to get a better understanding for the origin of this property, let us now calculate the viscous dissipation in the various regions of the bulk polymer, by estimating in each zone the value of the complex modulus: $\underline{\mu}(\omega) = \mu'(\omega) + i\mu''(\omega)$ (the different approximations are mentioned in Fig. 1). The crucial point here is that the integration of a *weak* loss modulus μ'' as in Eq.(12) over a *huge* volume can give rise to an energy enhancement comparable to the viscous region one. In Fig. 3, we present a simplified graphic representation of the regimes.

At *low separation rates*, $V < l/(\lambda\tau)$, the whole polymer material behaves as a "soft solid"; replacing μ' and $\mu''(\omega)$ by their approximated expressions in Eq.(12), we obtain:

$$\frac{G_v(V)}{G_0} \sim \frac{\lambda^2 V\tau}{l} \ \text{ for } \ V < \frac{l}{\lambda\tau}. \tag{13}$$

Thus, the (weak) loss modulus of the elastic region is sufficient to increase the fracture energy. The fracture energy reaches $G \sim \lambda G_0$ for a fracture speed as low as $V = l/(\lambda\tau)$, even if the "liquid zone" has not emerged yet.

For *intermediate separation rates* $[l/(\lambda\tau) < V < L/(\lambda\tau)]$, the "soft solid" region gives a dissipation of the same order as the liquid zone:

$$\frac{G_v(V)}{G_0} \sim \lambda \ \text{ for } \ \frac{l}{\lambda\tau} < V < \frac{L}{\lambda\tau}. \tag{14}$$

Finally, at *high separation rates* [for $V > L/(\lambda\tau)$], $G(V)$ is a decreasing function:

$$\frac{G_v(V)}{G_0} \sim \frac{L}{V\tau} \ \text{ for } \ V > \frac{L}{\lambda\tau}. \tag{15}$$

For uncrosslinked polymers, the rheological behavior is viscous at low frequencies: $\mu_0 = 0$ and the complex modulus can be written as:

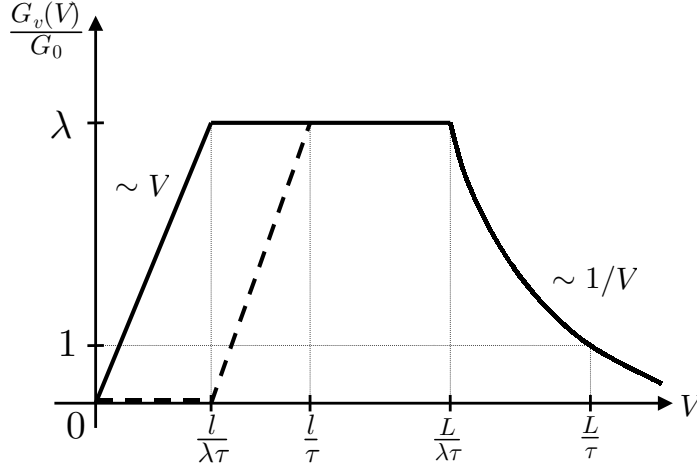$$\mu(\omega) = \mu_\infty \frac{i\omega\tau}{1 + i\omega\tau}. \tag{16}$$

Figure 3: Qualitative diagram of the viscous contribution G_v for fracture energy of a crosslinked polymer, versus separation rate V. The speed regime corresponding to Fig.2 is $l/\tau < V < L/(\lambda\tau)$ (plateau region with an enhancement λ of the adhesion energy). The limiting case $\lambda \to \infty$ of uncrosslinked polymers is characterized by the decreasing portion of curves ($G_v \sim 1/V$). For comparison, the dotted line represents the evolution of fracture energy as expected by earlier developpements[8, 9] : it is clear that the viscous amplification of adhesion begins at low separation rates, even in the absence of a real "liquid" zone ($V < l/\lambda\tau$).

Equation (23) thus gives:

$$\frac{G_v(V)}{G_0} \sim \frac{L}{V\tau}. \tag{17}$$

As expected, we recover the expression (15) for a crosslinked polymer at velocities V larger than $L/\lambda\tau$, *i.e.* when the soft solid region has disappeared because of the finite dimensions of the sample.

The adhesion energy expression (17) is compared with experiments in part 3.2.

2.3 The trumpet profile

If we assume the relation (5) between the distance to fracture tip and the frequency imponed to the material, we can relate the rheological properties of the material and the corresponding profile $u(x)$ in each region. In a linear approach of stress strain relations in the viscoelastic medium[28], the stress $\sigma(t)$ and strain $\gamma(t)$ are related by the relaxation modulus $G(t)$:

$$\sigma(t) = \int_{-\infty}^{t} G(t - \tau)\frac{\mathrm{d}\gamma(\tau)}{\mathrm{d}\tau}\mathrm{d}\tau. \tag{18}$$

If the strain history is specified as being a harmonic function of time according to $\underline{\gamma}(t) = \gamma_0 \exp i\omega t$ (with an amplitude γ_0), we can write:

$$\underline{\sigma}(t) = \underline{\mu}(\omega)\gamma_0 \exp^{i\omega t} = |\underline{\mu}(\omega)|\gamma_0 \exp^{i(\omega t + \tan^{-1}[\mu''(\omega)/\mu'(\omega)])}, \tag{19}$$

where $|\underline{\mu}(\omega)|$ is the magnitude of the complex modulus $\underline{\mu}(\omega)$. Taking the modulus of both sides of Eq.(19), we get:

$$|\underline{\sigma}(t)| = |\underline{\mu}(\omega)||\gamma_0|. \tag{20}$$

For a steadily growing mode I interface plane stress (or plane strain) crack under small scale yielding conditions, all field quantities are time independent with respect to an observer attached to the tip of the cohesive zone. Defining a polar coordinate system (r, θ) (cf. Fig. 2), we know[29] that the amplitude of stress inside an elastic material is given by:

$$\sigma_{ij}(r, \theta) = \frac{K_I}{\sqrt{2\pi r}} g_{ij}(\theta), \tag{21}$$

where K_I is the applied stress intensity factor[30] and $g_{ij}(\theta)$ are universal functions describing the angular variation of the crack tip stress field. In particular, the normal stress vanishes on the tip, but the other stress components follow the following scaling law with respect to the distance x to the crack tip:

$$\sigma(x) = \frac{K_I}{\sqrt{x}}. \tag{22}$$

Although we are dealing here with a complex viscoelastic medium, this simple scaling form (Eq.22) remains valid for our problem, as the equations of motion reduce in both cases to $\nabla\sigma = 0$, with identical compatibility conditions imposed to the stress components[31]. The strain imposed to a fluid element of length $\mathrm{d}x$ is simply given by $\gamma = \mathrm{d}u/\mathrm{d}x$. Relating x to ω by the scaling expression (5), we finally obtain:

$$\left| \mu\left(\omega = 2\pi\frac{V}{x} \right) \right| \cdot \frac{\mathrm{d}u}{\mathrm{d}x} = \frac{K_I}{\sqrt{x}}. \tag{23}$$

In each solid or liquid zone, we know from Eqs.(33) the expression of $|\mu| = \sqrt{\mu'^2 + \mu''^2}$, and can derive from Eq.(23) the expected profile $u(x)$[8].

In the *soft solid region*, where the frequencies are low ($\omega < 1/(\lambda\tau)$), we recover an elastic modulus: $|\mu| = \mu_0\sqrt{1 + (\lambda\omega\tau)^2} \approx \mu_0$. Equation (23) can be rewritten as: $\mu_0\mathrm{d}u = \sigma(x)\mathrm{d}x$, which simply traduces the linearity of displacement $\mathrm{d}u$ when a force $\sigma(x)\mathrm{d}x$ is exerted on the element $\mathrm{d}x$: the behavior is elastic, and we obtain from Eq.(23) the expected profile in region 1:

$$u_{\text{soft solid}} \sim x^{1/2}. \tag{24}$$

In the *liquid region*, in the same manner, we recover an viscous-type rheology, as $|\mu| = \mu_\infty\omega\tau\sqrt{1 + (\omega\tau)^2} \approx \mu_\infty\omega\tau$. Eq.(23) can be rewritten as: $\sigma = \eta\dot{\gamma}$, which is simply the stress constitutive relation for a Newtonian viscous fluid. Knowing that $|\mu| \sim 1/x$ in this zone, Eq.(23) gives the expected profile in region 2:

$$u_{\text{liquid}} \sim x^{3/2}. \tag{25}$$

The conclusions for the *strong solid region* are identical to the soft one. We predict:

$$u_{\text{strong solid}} \sim x^{1/2}. \tag{26}$$

Greenwood and Johnson[17] investigated the precise shape of the free surfaces of a crack, by using Barenblatt's approach[32]. Their conclusions agree with our qualitative picture of viscoelastic fracture: at very low speed, the crack has an elastic shape $u \sim x^{1/2}$ (*i.e.* the liquid zone has not emerged yet); at high speed, the profile is again purely elastic (*i.e.* the bulk of the material is only a strong solid zone); finally, at intermediate speeds, the three zones are present, including a central $u \sim x^{3/2}$ profile, whose extension depends on the form of the compliance function for the material.

These different velocity regimes are indeed experimentally observed (cf. Fig. 7), as developed below. Of course, the purely elastic shape at low velocity is not observed, as there is no elastic modulus at low strain-rates for an uncrosslinked polymer.

3 Experimental results

3.1 Experimental setup

In the experimental study, we chose to use an uncrosslinked polymer instead of a poorly crosslinked elastomer. The advantage is that such a liquid adhesive gives large enough deformations to be evidenced by simple optics set-up. Even if all the regimes discussed in the previous part will not be present in the experiments, the influence of viscous flow during failure was investigated in detail with in particular, the study of fracture profiles. This last point also required the use of thick adhesive layers in order to avoid additional cut-off length related to the thickness. The results presented below correspond to an adhesive thickness of 10 mm, larger than the diameter of the probe-adhesive contact area (about 6 mm). The adhesive we used is an uncrosslinked polydimethylsiloxane (PDMS) polymer (Rhodia, France) with a large molecular weight ($M_w = 497000$, $M_w/M_n = 1,9$). It exhibits model rheological properties and has a large characteristic time ($\tau = 0.6$ s) well suited to video recording rate.

The experimental procedure is detailed in[22] : we built a probe tack test experiment and adapted an optical set-up in order to visualize and measure the fracture profiles during the debonding process. This allowed to correlate the energy and stress measurements with the fracture propagation mechanism. An important point of our set-up is that we used a spherical probe (a glass watch). This was necessary to overcome the spurious problems of parallelism met with a flat probe. With the spherical one, the fracture always propagated symmetrically. This was nearly never the case with a flat probe. Note that a very small curvature is sufficient to guide the fracture radially : we used probes with a radius of curvature (about 10 cm) much larger than the observed deformations (about 1 mm) and than the radius of the probe-adhesive contact area (about 3 mm). As the characteristic angle of aperture of the probe (of order 3/100) is very small compared with the opening angle of fracture (of order 1/3), we therefore assumed that it did not modify the fracture mechanism compared with a flat probe. This spherical geometry is also very convenient to lighten and get sharp images. Another feature to note is that the velocity of the fracture measured on the video was constant during the propagation. The propagation speed increased only at the very end of the debonding. This is an important point in order to compare the results to the models developed at constant velocity. For every experiment we monitored the force F(t) during the debonding and deduced by numerical integration of this curve the adhesion energy per unit surface G. We also videotaped the fracture propagation. We
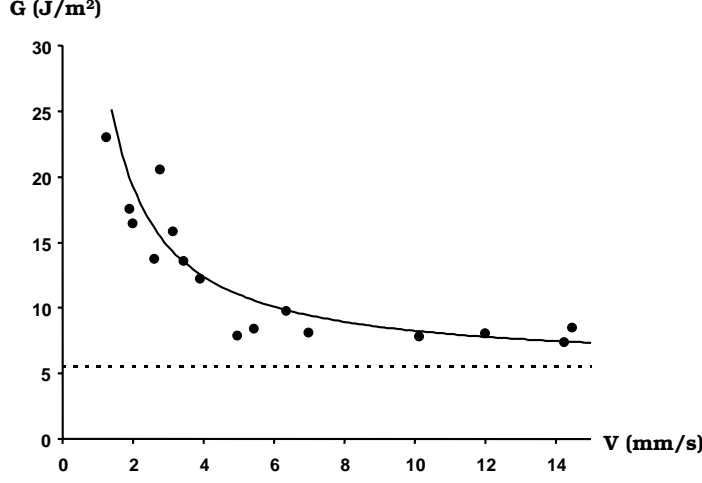
Figure 4: Adhesion energy G versus the fracture velocity V for a 10 mm-thick adhesive bond prepared during a contact time $T_c = 1$s and a contact pressure $P_c = 0,05$ N.m^{-2}. The dotted line represents the asymptotic value ($G = G_0$) reached by the fracture toughness at high separation rates. The solid curve corresponds to equation 27 with $L = 3$ mm, $\tau = 0.6$ s, and $G_0 = 5.5$ J.m^{-2}.

measured the fracture profile $u(x)$ as the distance between the polymer surface and the probe.

3.2 Adhesion energy G versus crack velocity

In the following we will consider only the case of adhesive failure when the bond breaks at the polymer-probe interface. At smaller separation velocities, the failure was cohesive as discussed in[22]. In Fig.4 we reported the adhesion energy of the bond as a function of the velocity V of propagation of the fracture. Note that the velocity V is different from the velocity at which the probe is withdrawn. Two regimes are clearly evidenced:

i) at large velocities, the energy G did not depend on the separation rate and tends towards a constant value. The fracture propagating at the adhesive-probe interface was very rapid so that the polymer has no time to flow: it has an elastic behavior. In this case the constant energy value is governed by processes occurring close to the fracture tip.

ii) for smaller velocities the failure was still interfacial but the energies measured are larger. As shown in[22] this energy enhancement is caused by viscous losses in the bulk of the polymer far from the fracture tip. The fracture is slow enough to let the polymer flow.

We compared the energy measurements reported in Fig.4 with the model described above. From Eq.(17) we deduced the expression of the fracture energy :

$$G = G_0 \left(1 + \frac{L}{V\tau} \right). \tag{27}$$

As shown in Fig.4 this expression describes very well the energy measurements. The energy enhancement appeared for fracture velocities lower of 5 mm·s^{-1} which is in very good agreement with the expected value $V = L/\tau$. In our experiment $L \sim 3$ mm, $\tau \sim 0.6$ s which gives $V \sim 5$ mm·s^{-1}. Using these values we deduced from the fit the value of $G_0 = 5.5$ J·m^{-2}.
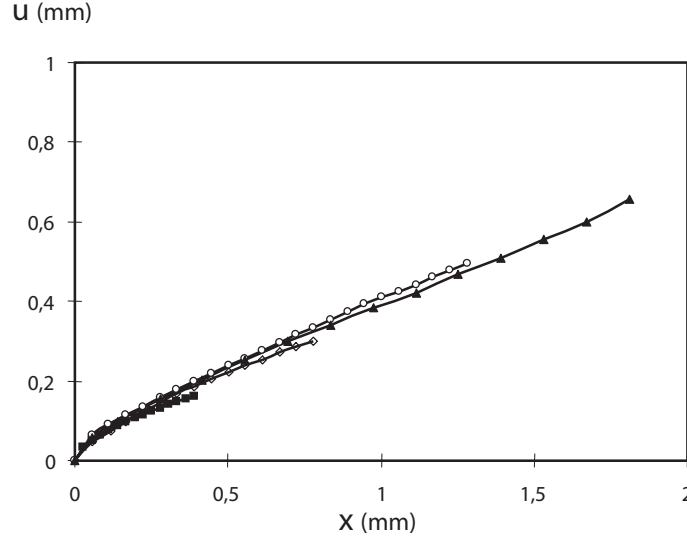
10

Figure 5: Fracture profiles $u(x)$ in the moving frame at different times ($\blacksquare$ $t = 0.2$s, $\diamond$ $t = 0.4$s, $\circ$ $t = 0.6$s, $\blacktriangle$ $t = 0.9$s; $t = 0$ corresponds to the beginning of crack propagation) during one debonding experiment ($V = 2$ mm·s^{-1}, $G = 3\,G_0$)

3.3 Fracture profiles

The fracture profiles measured in the moving frame during an experiment at V $= 2$ mm·s^{-1} corresponding to the viscoelastic regime are represented in Fig.5 . At the beginning of the propagation the profile was parabolic $u \sim x^{1/2}$ as evidenced in the logarithmic representation (Fig.6). As the propagation proceeded we noted an important modification of the profile : close to the fracture tip the profile is still parabolic but we observe a change in the concavity of the profile far from the fracture tip. For x larger than about 1 mm the profile is described by a power law larger than 1/2. This distance is in good agreement with the $L \sim V\tau = 1.2$ mm distance expected in the theoretical part as the transition between solid and liquid zones. All these profiles coming from a single experiment corresponds qualitatively to the trumpet profile discussed in detail above.

It was then interesting to compare profiles of experiments coming from the two distinct regimes : elastic and viscoelastic. In Fig.7, we superposed two profiles obtained at about 2/3 of the fracture propagation for an experiment in the elastic regime ($V = 14.5$ mm·s^{-1}, $G = 1.3G_0$) and an experiment in the viscoelastic regime ($V = 3.9$ mm·s^{-1}, $G = 2.2\,G_0$). This latter profile is similar to the ones reported in Fig.5 except that the transition from elastic to viscous profile occurs for a larger distance $x \sim 2$ mm which is still in good agreement with the $L \sim V\tau = 2.3$ mm value. As for the profile in the elastic regime, the profiles are identical close to the fracture tip but differ in the far field region. In the elastic case the fracture propagation is so rapid that the polymer remains elastic. The value of $L \sim V\tau = 8.7$ mm is larger than the contact size. During all the propagation the fracture profile is described by the parabolic profile $u \sim x^{1/2}$ (see Fig.8). The difference between the two curves of Fig.7 materializes the viscous flow which is responsible for the energy enhancement obtained in the viscoelastic regime.
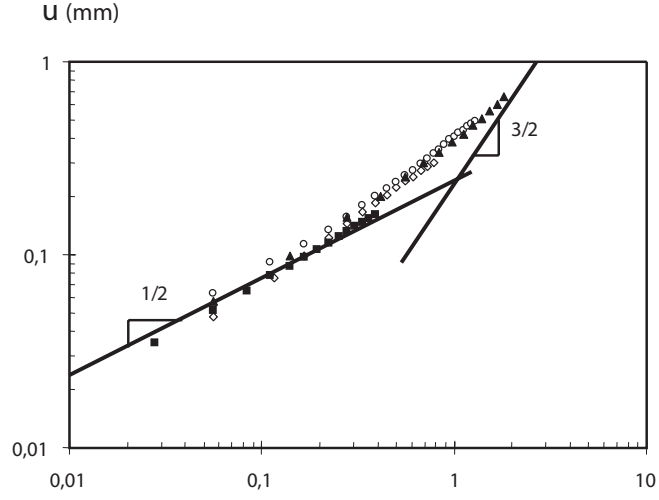
Figure 6: Fracture profiles $u(x)$ in the moving frame at different times (cf. Fig.5) during one debonding experiment ($V = 2$ mm·s^{-1}, $G = 3\,G_0$), in logarithmic scale. The two black lines represent the power laws $u \sim x^{1/2}$ and $u \sim x^{3/2}$.
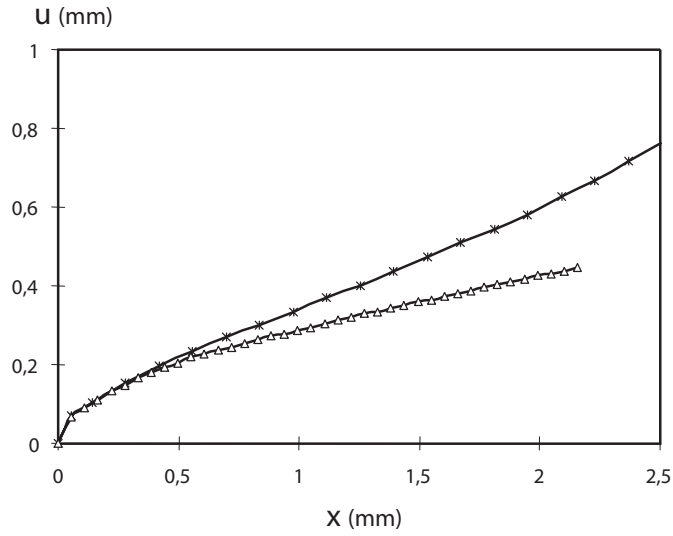

Figure 7: Fracture profiles $u(x)$ in the moving frame corresponding to different experiments : (✳) experiment in the viscoelastic regime $V = 3.9$ mm·s^{-1}, $G = 2.2\,G_0$; (△) experiment in the elastic regime $V = 14.5$ mm·s^{-1}, $G = 1.3\,G_0$.
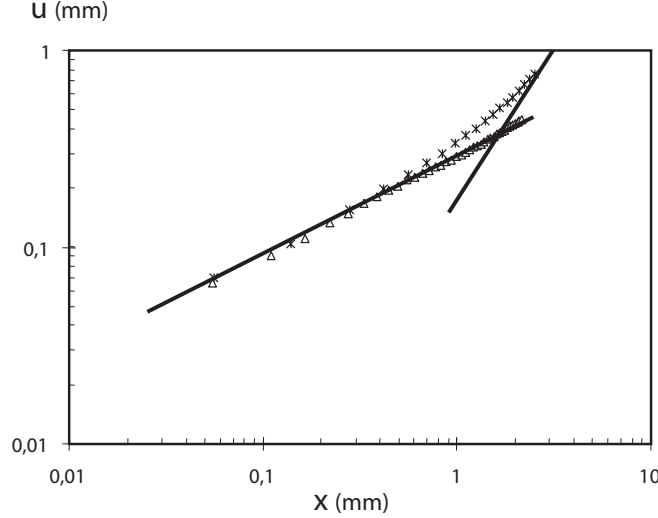
12

Figure 8: Fracture profiles $u(x)$ in the moving frame corresponding to different experiments, in logarithmic scale: ($*$) experiment in the viscoelastic regime $V = 3.9$ mm·s^{-1}, $G = 2.2\,G_0$; ($\triangle$) experiment in the elastic regime $V = 14.5$ mm·s^{-1}, $G = 1.3\,G_0$. As in Fig.6, the black lines represent the power laws $u \sim x^{1/2}$ and $u \sim x^{3/2}$.

All these results verify qualitatively the picture of the trumpet profile schematized in Fig.2 (except for the soft solid zone which is not present with a liquid polymer). However, the range of distances available experimentally was not sufficient to clearly observe the $u \sim x^{3/2}$ characteristic of the liquid zone. We only observed a transition regime that can be large because, in such systems, the transition between solid and liquid behavior extends over several orders of magnitude of solicitation rate.

In order to make more quantitative comparison we tried to fit the fracture profiles with Eq.(23) which gives a direct relation between the fracture profile $u(x)$ and the rheological property $|\mu(\omega)|$ of the adhesive. The rheological data $\mu'(\omega)$ and $\mu''(\omega)$ were measured using a Rheometrix RDA2 machine. For each point of the profile, we calculated the corresponding pulsation $\omega = 2\pi V/x$ where V is the fracture velocity and determined the corresponding modulus $|\mu(\omega)|$. The profiles $u(x)$ were determined as explained above. We tested two methods to derivate the profiles: a numerical derivation or a fit by a polynomial function followed by an analytical derivation. These two methods gave the same results within a 10% uncertainty. We preferred the numerical method because the polynomial fit was not perfect close to the fracture tip.

In Fig.9 we reported, for every profile of Figs.5 and 7 the value of $|\mu(\omega)| \cdot du/dx$ as a function of x. We observe that the curves corresponding to the different profiles fit on a same curve. The parabolic profiles of Fig.5 observed at the beginning of the propagation as well as the "trumpet" profiles that develop after a given time give the same power law in this representation. It is also the case for the profiles of Fig.7 coming from different types of fracture propagation. In fact, Eq.(23) holds for all conditions of solicitation. The stress intensity factor K_I characterizes the
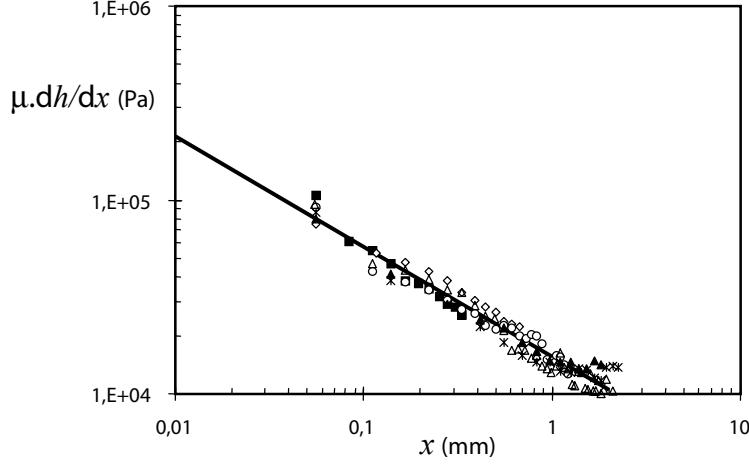
13

Figure 9: $|\mu(\omega)| \cdot du/dx$ versus x for the six profiles reported in Figs.5 and 7. The symbols used are identical to those used in Figs.5 and 7. The black line is the best power-law fit: $|\mu(\omega)| \cdot du/dx \sim x^{-0.56}$.

strength of the bond and is directly related to G_0 by:

$$G_0 = \frac{K_I^2}{\mu_\infty}. \tag{28}$$

Both parameters G_0 and K_I describe processes occurring at the fracture tip and therefore depend only on the preparation of the bond. All the experiments of Fig.4 thus correspond to a same value of K_I. The far field losses induced an enhancement of the energy in the viscoelastic regime but did not modify the stress distribution in the adhesive. For that reason, the profiles of Figs.5-8, in the elastic as well as in the viscoelastic regimes, coincide in the representation $|\mu(\omega)| \cdot du/dx$ versus x. The power law deduced from Fig.9 is $|\mu(\omega)| \cdot du/dx \sim x^{-0.56}$ in rather good agreement with the $x^{-1/2}$ expected from Eq.(23). The deduced value of the stress intensity factor is $K_I = 18000$ N·m$^{-3/2}$. The value $G_0 = 3$ J·m^{-2} deduced from the profiles according to Eq.(28) is of the order of the value $G_0 = 5.5$ J·m^{-2} deduced from adhesion energy measurements.

All these experimental results validate the picture of the trumpet profile and its influence on the adhesion energy of a viscoelastic polymer.

4 Conclusion and perspectives

In conclusion, we proposed a qualitative description of the dissipative processes occurring during the failure of the interface between a viscoelastic material and a solid substrate, mainly based on de Gennes' initial approach[9]. In particular, we analyzed the enhancement of fracture energy due to far-field viscous dissipation in the bulk material. The results of our scaling analysis are in accordance with the more rigorous ones of Hui *et al.*[10] and Greenwood *et al.*[17].

We have shown that, for a crosslinked elastomer, the interface toughness $G(V)$ starts from a relatively low value G_0 due to local dissipative processes near the crack tip, and reaches a maximum of order $G_0(\mu_\infty/\mu_0)$ (see eq.2). It was shown that our simple model accounts well

14

for the dependence of fracture energy $G(V)$ for a polymer melt, for which the fracture energy should scale as $1/V$. The two velocity regimes, and the peculiar crack profiles experimentally observed validate our description in two zones: an elastic region near the crack tip, and a liquid zone with a different concavity at distances larger than $V\tau$ (where the material had enough time to flow).

The "viscoelastic trumpet" model[9] is thus a simple, tractable, linear model which describes well, on the basis of viscoelasticity, the viscous origin of fracture energy enhancement observed in many systems. Our aim here is to point out that the fracture energy originating from viscous dissipation in the bulk polymer had been underestimated at low velocities. Some experiments measuring the quantity G_0 for elastomers, by taking a crack velocity as small as practically possible, which obtain too large values for G_0, may thus be reassessed by taking into account the viscous dissipation existing in large volumes of soft elastic regions.

To conclude, let us insist on the fact that this "viscoelastic trumpet" model is a qualitative approach of a very complex phenomenon, and lies on many approximations: in particular, the independence versus V of the adhesive zone scale l, and of the associated dissipation term G_0, is obviously discutable as it has been proved that for many systems G_0 exhibits a marked dependence on V, and most of the rate dependence of $G(V)$ then originates from the rate dependence of G_0 itself[4]. We can thus expect our model to apply to systems characterized by a relatively weak adhesion, for which G_0 (and subsequently l) is effectively quasi-independent on V: this is the case of the very high molecular weight PDMS studied in the experimental section (at short times, or high separation rates, this type of material behaves elastically and does not dissipate much near the crack tip, as a consequence of its very low glass transition temperature). Most of other uncrosslinked systems are characterized by an increasing dissipation with increasing velocity, even in the elastic regime[39–42], because the increase in G_0 dominates when the adhesion hysteresis is large and the material is soft, even when the polymer is macroscopically elastic[43]. A more realistic description of the microscopic processes taking place in the adhesive zone, including nonlinear effects and specific properties like crack blunting[44] for very soft materials (characterized by a weak elastic modulus $E \lesssim 0.1$ MPa), represents a theoretical challenge, and a possible further extension of our simplistic model.

5   Acknowledgements

A   Analytical results for crosslinked and uncrosslinked polymers

This appendix provides the main analytical results about the fracture energy derived from the integral expression (12) of $G(V)$. We will discuss both cases of crosslinked and uncrosslinked polymers, whose corresponding mechanical models are represented in Fig.10.
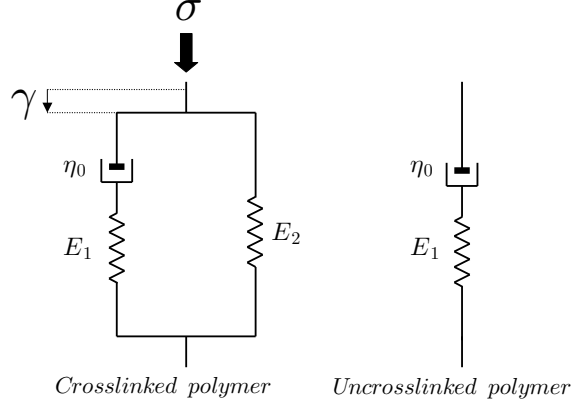
Figure 10: Rheological models for (i) crosslinked and (ii) uncrosslinked polymers. **(i)** The mechanical analog for a crosslinked material (Zener's model) consists in the association of two springs (with moduli E_1 and E_2), with a dashpot of viscosity η. **(ii)** When the second spring (of modulus E_2) is removed, we find back a liquid-like material (Maxwell's model), which can figure the rheology of a uncrosslinked polymer melt.

A.1 Rheological characteristics

To begin with, let us find back the expressions (2) and (16) of the complex modulus for both cases. Following the notations E_1, E_2 and η introduced in Fig.10, it can easily be shown that the applied stress σ and the strain γ are related by the following differential equation:

$$\sigma + \frac{\eta_0}{E_1}\dot{\sigma} = E_2\varepsilon + \eta_0\frac{E_1 + E_2}{E_1}\dot{\varepsilon} \tag{29}$$

The prefactor η_0/E_1 is a characteristic time of the material, denoted $\tau = \eta_0/E_1$.

$$\underline{\sigma} = \left(E_2 + E_1\frac{i\omega\tau}{1 + i\omega\tau}\right)\underline{\gamma} \tag{30}$$

Defining the two parameters μ_0 and μ_∞ as $E_1 \equiv \mu_\infty - \mu_0$ and $E_2 \equiv \mu_0$, we thus obtain the expression (2) of the complex modulus:

$$\underline{\mu}(\omega) = \mu_0 + (\mu_\infty - \mu_0)\frac{i\omega\tau}{1 + i\omega\tau}. \tag{31}$$

In the same way, the rheological behavior of an uncrosslinked polymer, whose corresponding mechanical model is represented in Fig.10, can be described by the following complex modulus:

$$\mu(\omega) = \mu_\infty\frac{i\omega\tau}{1 + i\omega\tau}. \tag{32}$$

16

A.2 Fracture energy $G(V)$ derived from the integral expression Eq.12

A.2.1 Analytical results for an elastomer

It is straightforward to see that for the rheological law (2), one has:

$$\begin{cases} \mu'(\omega) = \mu_0 + (\mu_\infty - \mu_0)\frac{\omega^2\tau^2}{1+\omega^2\tau^2}, \\ \mu''(\omega) = (\mu_\infty - \mu_0)\frac{\omega\tau}{1+\omega^2\tau^2}. \end{cases} \tag{33}$$

According to Eq.12, this leads to:

$$\frac{G_v(V)}{G_0} \cong \frac{\mu_\infty(\mu_\infty - \mu_0)}{\mu_0^2}\tau \int_{V/L}^{V/l} \frac{\mathrm{d}\omega}{1 + \lambda^2\omega^2\tau^2}, \tag{34}$$

that is:

$$\frac{G_v(V)}{G_0} \cong (\lambda - 1)\left[\arctan\left(\frac{\lambda V\tau}{l}\right) - \arctan\left(\frac{\lambda V\tau}{L}\right)\right]. \tag{35}$$

As pointed out before, the viscoelastic effect gives a multiplicative enhancement of the energy G_0 dissipated by local processes in the adhesive zone. The multiplicative factor, of order $\lambda = \mu_\infty/\mu_0$, depends on the degree of cross-linking: a higher crosslinkage induces an increase in μ_0 and therefore a decrease in energy of adhesion, as shown by Gent and Petrich[27]. We have already mentioned that a large ratio λ can be experimentally achieved, to give rise to a good viscous amplification of the adhesion energy.

In Fig.11 we present a logarithmic representation of the fracture energy versus the dimensionless separation rate $\lambda V\tau/l$. The fracture toughness $G(V)$ exhibits a maximum for a separation rate V^* given by:

$$V^* = \frac{\sqrt{lL}}{\lambda\tau}. \tag{36}$$

The adhesion energy is maximal for $V = V^*$, where it takes the value:

$$G_{max} = G_0\left(1 + (\lambda - 1)\left[\arctan\left(\sqrt{\frac{L}{l}}\right) - \arctan\left(\sqrt{\frac{l}{L}}\right)\right]\right). \tag{37}$$

A.2.2 Analytical results for a polymer melt

For uncrosslinked polymers, characterized by the complex modulus (16), equation (23) gives:

$$\frac{G_v(V)}{G_0} \sim \frac{L - l}{V\tau}. \tag{38}$$

Provided that the length l of the adhesion zone remains small compared with the whole sample dimension L, we recover the expression 15 for a crosslinked polymer at velocities V larger than $L/\lambda\tau$, *i.e.* when the soft solid region has disappeared because of the finite dimensions of the sample :

$$\frac{G_v(V)}{G_0} \sim \frac{L}{V\tau}. \tag{39}$$

The adhesion energy expression (17) is compared with experiments in part 3.2.
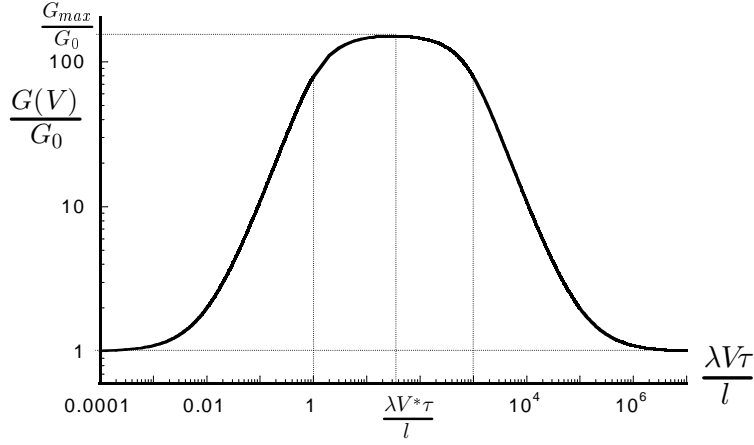
Figure 11: Fracture energy $G(V) = G_0 + G_v(V)$ versus separation rate V, according to Eq.(35) with Zener's model. This logarithmic representation clearly exhibits the plateau region with an enhancement of order λ of the adhesion energy G_0. The curve has a maximum G_{max} obtained for $V = V^*$. The ratios $L/l = 1000$ and $\lambda = 100$ were chosen for this graphic representation.

References

[1] Brown, H. *Physics World* **1996** , *Jan.*, 38.

[2] Jones, R. A. L. ; Richards, R. W. *Polymers at surfaces and interfaces*; Cambridge Univ. Press, 1999.

[3] C. Creton, C; Kramer, E. J.; Brown, H. R.; Hui, C.-Y. *Adv. Polym. Sci.* **2001**, *156*, 53.

[4] Gent, A. N. *Langmuir* **1996**, *12*, 4492.

[5] Gent A. N. ; Shultz J, *J. Adhesion*, **1972**, *3*, 281.

[6] Andrews E. H.; Kinloch A. J. *Proc. Roy. Soc. (Lond.)* **1973** *A332 385*, 401.

[7] Williams, M. L. ; Landel, R. F.; Ferry, J. D.; *J. Am. Chem. Soc.* **1995** *77*, 3701.

[8] de Gennes, P.-G. *C. R. Acad. Sci. Paris* **1988**, *307*, 1949.

[9] de Gennes, P.-G. *Langmuir* **1996**, *12*, 4497.

[10] Hui, C.-Y. ; Xu, D.-B.; Kramer, E. J. *J. Appl. Phys.* **1992**, *72*, 3294.

[11] Christensen R. M.; Wu, E. M. *Engineering Fracture Mechanics* **1981**, *14*, 215.

[12] Bowen J.M.; Knauss, W. G. *J. Adhes.* **1992**, *39*, 43.

[13] Christensen, R. M. *Int. J. Fracture* **1979** *15*, 3.

[14] Schapery, R. A. *Int. J. Fracture* **1975** *11*, 141; Schapery, R. A. *Int. J. Fracture* **1975**, *11*, 369; Schapery, R.A. *Int. J. Fracture*, *11*, 549.

[15] Freund, L. B.; Hutchinson, J. W. *J. Mech. Phys. Solids* **1985** *33*, 169.

[16] Barber M.; Donley J.; LangerJ. S. *Phys. Rev. A* **1989** *40*, 366.

[17] Greenwood, J. A.; Johnson K. L. *Phil. Mag. A.* **1981** *43*, 697.

[18] de Gennes, P.-G. *C. R. Acad. Sci. Paris* **1991** *3*12, 1415.

[19] Gent A. N.; H. J. Kim H. J. *Rubber Chem. Tech.* **1990**, *63*, 613.

[20] Creton, C; Leibler, L. *J. Polym. Sci. B* **1996** *3*4, 545.

[21] Gay, C.; Leibler *Physics Today*, **1999**, *Nov* 48 ; see also references therein.

[22] Ondarçuhu, T. *J. Phys. II France*, **1997**, *7*, 1893.

[23] Equation 2 corresponds to a Zener model with a *single* relaxation time τ. The latter assumption is rather crude, as the dangling ends have a wide distribution of length, etc., but allows a clear representation of the different spatial zones far behind the fracture tip.

[24] Gent A. N.; Lai, S.-M. *J. Polym. Sci. B* **1994**, *32*, 1543.

[25] More precisely, L is the overall length of the solicitated region. For instance, if the viscoelastic material is in the form of a thin slab of thickness w, then $L \sim w$.

[26] Various phenomena may occur in the adhesive zone[33], *e.g.* chain pull-out[34,35]. In refs.[10,36], the material in the adhesive zone is described a newtonian fluid with a cut-off stress required for the interface to initiate an opening displacement. The precise description of the adhesive zone will not be considered here[37,38].

[27] Gent A. N.; Petrich, R. *Proc. R. Soc. London* **1969**, *A*31, 433.

[28] Christensen R. M. *Theory of viscoelasticity, an introduction*, Academic Press, 2nd edition, 1982.

[29] Rice J. R., *Fracture II, an Advanced Treatise*, H. Liebowitz ed., Academic Press, New York, 1968.

[30] H. Tada, P. C. Paris, and G. R. Irwin, *The stress analysis of cracks Handbook* del Research, Hellertown, 1973.

[31] de Gennes, P.-G. *Soft Interfaces* Cambridge Univ. Press, 1997.

[32] Barenblatt G. I. *Adv. Appl. Mech.* **1962** *7*, 55.

[33] de Gennes, P.-G. *Can. J. Phys.* **1990**, *6*8, 1049.

[34] Creton, C; Brown, H. R.; Schull K. R. *Macromol.* **1994** *2*7, 3174.

[35] Léger, L; Raphaël, E; Hervet, H. *Adv. in Polym. Sci.* **1999** *138*, 185.

[36] Raphaël, E; de Gennes P.-G. *J. Phys. Chem.* **1992** *96*, 4002.

[37] Marciano, Y.; Raphaël, E. *Int. J. Fracture* **1994** , *67*, 23.

[38] Xu, D.-B.; Hui, C.-Y.; Kramer, E. J.; Creton, C. *Mechanics of Materials* **1991**, *11*, 257.

[39] Benyahia, L.; Verdier, C; Piau, J. M. *J. Adhes.* **1997**, *62*, 45.

[40] Derail, C; Allal, A.; Marin, G.; Tordjeman, P. *J. Adhes.* **1997** *61*, 123.

[41] Christensen, S. F. ; Everland, H.; Hassager, O.; Almdal, K. *Int. J. Adhesion and Adhesives* **1998** *18*, 131.

[42] Christensen, S. F. ; Flint, S. C. *J. Adhes.* **2000**, *72*, 177.

[43] Maugis, D; Barquins, M. *J. Phys. D: Appl. Phys.* **1978**, *11*, 1989.

[44] Hui, C.-Y.; Jagota, A; Bennison, S. J.; Londono, J. D. *Proc. Royal Soc. London, Ser. A: Mathematical and physical sciences* **2003** *403*, 1489.